Fault diagnosis and fault-tolerant control in wave energy: A perspective

Proc. of the International Conference on Electrical, Computer, Communications and Mechatronics Engineering (ICECCME 2025)
16-19 October 2025, Zanzibar, Tanzania

Design Methodology of a Pneumatic Force-Control Servo System for a Ball Screw Test Bench

Antonio Carlo Bertolino*
Department of mechanical and aerospace engineering
Politecnico di Torino
Torino, Italy
antonio.bertolino@polito.it

Andrea De Martin
Department of mechanical and aerospace engineering
Politecnico di Torino
Torino, Italy
andrea.demartin@polito.it

Massimo Sorli
Department of mechanical and aerospace engineering
Politecnico di Torino
Torino, Italy
massimo.sorli@polito.it

***Abstract*—Force control in pneumatic systems is particularly challenging due to the strong nonlinearities and the compressibility of air. To support the preliminary design of the control architecture, simple, fast, yet accurate linearized models are required before moving to detailed nonlinear analyses for final tuning. This paper presents the derivation and validation of a design methodology for a pneumatic force-controlled servo system, applied to a novel test bench for ball screw characterization, where an electromechanical actuator and a pneumatic force-control system are coupled to reproduce realistic load conditions. A fully parametric linearized model is developed to support early-stage design and control synthesis. Its performance is assessed by comparison with a high-fidelity nonlinear model, showing strong predictive capabilities and excellent agreement in the frequency response across a broad range of operating frequencies.**

***Index Terms*—Pneumatic servosystem, Closed loop force control, Linear model, Servosystem design**

I. Introduction

Pneumatic systems represent an extremely dynamic field of research, with the potential to replace hydraulic or electromechanical systems in different applications. Pneumatic systems offer numerous advantages, including high compactness, especially when using rodless actuators, high power-to-weight ratio, and reliability. In addition, they require reduced maintenance and, thanks to a high degree of standardization and ease of assembly, enable the development of modular systems. Air-powered actuation is also valued for the nature of the working fluid, making it a safe and clean technology. These aspects make them attractive for mechatronic applications, especially those focused on position and speed control.

The pneumatic solution is less frequent in those applications requiring dynamic force control, because of the presence of strong non-linearities. Unlike traditional position or velocity-controlled pneumatic systems, force-controlled systems aim to directly regulate the interaction force between the actuator and the environment.The inherent challenges of force control in pneumatic systems stem from the compressibility of air, nonlinear flow dynamics, and frictional effects, making accurate force regulation complex [1]. Starting from modified PID control [2], [3], advanced control strategies, including adaptive control [4], model predictive control (MPC), and so forth, are often employed to improve force tracking performance [5]. Additionally, integrating pressure sensors and force transducers enables real-time feedback, allowing for more precise and stable force control [6].

Accurate force control, therefore, requires a high-fidelity modeling of the system to correctly capture and study the various effects influencing the overall behavior, including air compressibility, flow dynamics, and mechanical nonlinearities. At the same time, it is equally necessary to develop a simple, fast, yet accurate linearized framework of the servosystem, which allows for an early-stage design and performance analysis and the preliminary setup of the control strategy.

The objective of this paper is precisely to address these needs by deriving a linearized model of a force-controlled pneumatic servosystem, which is installed on a dedicated test bench currently under development in our laboratories [6].

II. Test bench architecture

The research presented in this paper originates from the development of a test bench designed to study ball screws, whose architecture is schematically depicted in Fig. 1.

The test bench is composed of an electromechanical actuator (EMA) and an opposing force-controlled pneumatic actuator. The EMA drives a sled via a ball screw mechanism, converting motor rotation into linear motion. The sled holds the ball screw nuts and is guided by low-friction linear rails to prevent undesired rotations. An innovative dual-nut configuration allows the application and fine adjustment of a controlled preload on the ball screw, dynamically measured by a load cell. The master nut sustains the external load generated by the pneumatic actuator, while the slave nut adjusts the preload through a spring-based mechanism. The EMA is controlled in position or speed through a motor driver, using feedback from both

Funding: The work was funded by the Power Electronics Innovation Center of Politecnico di Torino.
* Lead and contact author: antonio.bertolino@polito.it

979-8-3315-3556-8/25/$31.00

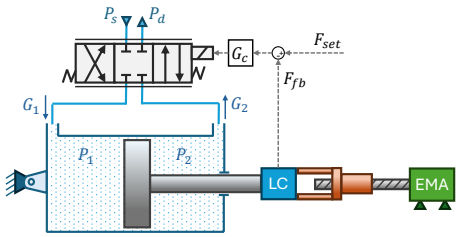

Fig. 1: Schematic representation of the test bench's pneumatic force-controlled servosystem.

an internal resolver and an external linear encoder to ensure precise motion control. Torque and angular speed at the ball screw input are measured by a non-contact torque sensor.

The pneumatic actuator applies a variable external force through a proportional flow valve and a closed-loop force control system, supported by pressure sensors and an accumulator to ensure stable operation even under fast transients.

The test bench includes an extensive sensor suite, enabling dynamic model validation, health monitoring studies, and the characterization of ball screw behavior under different load and speed conditions. More details can be found in [6].

III. Pneumatic Servosystem Model

This section describes the various equations needed to create a mathematical model of the pneumatic part of the test bench described in Section II. To facilitate the mathematical modeling, the actual test bench architecture has been simplified and approximated to a standard layout, as illustrated in Figure 1. Only the main components, i.e. the servovalve, the cylinder, the load cell and the controller, have been considered at this stage, while secondary elements have been deliberately omitted as they would unnecessarily complicate the analysis without introducing significant changes to the system response. These elements will be progressively incorporated in the following phases, as the model evolves toward higher fidelity.

The pneumatic servovalve receives the voltage reference signal from the regulator, which controls the spool position and, consequently, regulates the opening and closing of the internal flow section in both supply and discharge modes. To formulate a dynamic model capable of relating the valve flow rate to the input reference signal under varying port pressure conditions, it is expedient to consider the valve as composed of distinct subsystems: namely, the electrical and electromagnetic circuits and magnetic force generation, the spool's mechanical actuation including equilibrium, spring, and end-stroke constraints, and the pneumatic regulation of the mass flow rate [7]. The latter is assumed to be governed solely by resistive effects, expressed as a function of the spool displacement and the pressures at the valve ports, i.e. the supply and discharge absolute pressures P_s and P_d, and the cylinder's chamber absolute pressures P_1 and P_2.

In accordance with the international standard ISO 6358 [8], which characterizes the mass-flow-rate equation as an elliptic equation, the mass flow rate of air passing through the valve can be described as the flow rate through a throttle orifice:

$$G_j = \rho_{ANR} P_s C\left(V_{ref}\right) \sqrt{\frac{T_{ANR}}{T_s}}\, \Psi\left(P_j, P_s, P_d\right)$$
$$\Psi = \begin{cases} \sqrt{1-\left(\frac{\frac{P_1}{P_s}-b}{1-b}\right)^2} & \text{if} \quad j=1 \ \wedge \ bP_s \le P_1 \le P_s \\ \sqrt{1-\left(\frac{\frac{P_d}{P_2}-b}{1-b}\right)^2} & \text{if} \quad j=2 \ \wedge \ P_d \le P_2 \le \frac{P_d}{b} \\ 1 & \text{otherwise}\,(j=1,2) \end{cases} \tag{1}$$

where C is the valve's sonic conductance, dependent on the reference voltage V_{ref}, b is the critical pressure ratio of the valve ($b < 0.528$), ρ_{ANR} and T_{ANR} represent the density and absolute temperature at the predefined normal reference conditions, as specified by ISO standards, with $T_{ANR} = 293.15$ K, $P_{ANR} = 101325$ Pa, and $\rho_{ANR} = 1.2$ kg/m^3 for a relative humidity of 65%. The corresponding gas constant is given as $R = 287.5$ J/(kg K). Equation (1) only describes the flow rates under the assumptions of $P_d \le P_j \le P_s$ with $j = 1{,}2$.

The flow rates G_j ($j = 1{,}2$) passing through the servovalve's ports are considered directly entering the cylinder's chambers according to the sign convention depicted in Fig. 1, disregarding servovalve's internal leakages and resistive and capacitive effects of the pipes connecting these two elements. The continuity equation of the rear chamber (Chamber 1) of the cylinder can thus be described as follows:

$$G_1 = \frac{dM_1}{dt} = \frac{d\rho_1 V_1}{dt} = V_1 \frac{d\rho_1}{dt} + \rho_1 \frac{dV_1}{dt} \tag{2}$$

with the volume of Chamber 1 expressed as $V_1 = A_1(x_0 + x_m + x)$, in which A_1 is the active piston area of the Chamber 1, x_0 is the initial rod displacement, x_m is the equivalent rod displacement associated with the dead volume of Chamber 1 and x is the current rod coordinate, considering as reference the mid-stroke position.

The same equation can be written for the Chamber 2, with $V_2 = A_2(x_0 + x_m - x)$, as follows:

$$-G_2 = \frac{dM_2}{dt} = \frac{d\rho_2 V_2}{dt} = V_2 \frac{d\rho_2}{dt} + \rho_2 \frac{dV_2}{dt} \tag{3}$$

The minus sign comes from the assumption of assuming as positive the flow exiting Chamber 2, as depicted in Fig. 1.

Under the assumption of perfect gas, the densities of the air in the two chambers, respectively ρ_1 and ρ_2, are linked to temperatures and pressures according to the gas state equation $P_j/\rho_j = RT_j$. If a polytropic transformation $P\,\rho_i^n = P_i\,\rho^n$ is assumed for the air within each chamber of the cylinder, the continuity equations (2) and (3) of the cylinder's chambers can be rewritten as:

$$G_1 = +\frac{A_1\left(x_0 + x_m + x\right)}{nRT_{1i}} \left(\frac{P_1}{P_{1i}}\right)^{\frac{1}{n}-1} \frac{dP_1}{dt} + \frac{P_1 A_1}{RT_{1i}} \frac{dx}{dt} \tag{4}$$

$$G_2 = -\frac{A_2\left(x_0 + x_m - x\right)}{nRT_{2i}} \left(\frac{P_2}{P_{2i}}\right)^{\frac{1}{n}-1} \frac{dP_2}{dt} + \frac{P_2 A_2}{RT_{2i}} \frac{dx}{dt} \tag{5}$$

where the subscript i identifies initial conditions, and $1 \leq n \leq 1.4$, with $n = 1$ representing an isotermal transformation and $n = 1.4$ an adiabatic transformation.

The difference between the two chamber's pressures determines the generation of the requested force F_e according to the dynamic equilibrium equation:

$$P_1 A_1 - P_2 A_2 - P_{amb}(A_1 - A_2) - M\ddot{x} - \gamma\dot{x} - F_{fr} - F_e = 0 \tag{6}$$

where P_{amb} is the ambient absolute pressure, M is the equivalent mass of the moving parts connected to the rod, γ is the damping coefficient and F_{fr} represents the friction between the rod and the cylinder. The speed of the rod, controlled by the electro-mechanical position-controlled part of the test bench, acts as external disturbance on the force control system.

The force read by the load cell is conditioned and used as feedback to close the control loop. The mathematical model of the controller considers all the various delays associated with the acquisition of the signals, computation of the reference setpoint and generation of the output voltage for the servovalve.

IV. Model linearization

The non-linear model described in the previous section has been used to generate representative responses under various operating conditions and will serve as a reference for validating the linearized model. However, for the purposes of both the test bench design and, more importantly, the control algorithm development, a linearized representation of the system is required.

Linearization provides a simplified yet insightful approximation of the system dynamics in the vicinity of a specific operating point, enabling the application of classical control techniques and facilitating the analysis of stability, robustness, and performance. This section presents the procedure adopted to obtain the linearized model, discusses the selection of the operating point, and outlines the main assumptions and limitations involved in the process.

Particular attention has been paid to the servovalve, which represents the most significant source of non-linearity within the system, especially in the subsonic region, and has therefore been the main focus of the linearization process. As previously stated, the servovalve is modeled as two variable-section orifice, whose effective area depends on the spool displacement x_v. It is assumed that the spool position connects the rear chamber (Chamber 1) to the supply port, allowing it to be pressurized, while the front chamber (Chamber 2) is vented to the atmosphere.

The assumption of symmetric ports, critical lap, no leakages and same function of cross sectional area with the spool displacement, can be summarized in the following expressions for the valve conductance:

$$\begin{cases} C_{(s\to 1)} = C_{(2\to d)} & x_v > 0 \\ C_{(1\to d)} = C_{(s\to 2)} & x_v < 0 \\ C_{(s\to j)} = C_{(j\to d)} & x_v = 0 \quad \forall j \end{cases} \tag{7}$$

which is basically a simplification of the usual representation of the servovalve flow rate by means of the electrical domain analogy of the Wheatstone bridge [7], [9], [10]. From this point onward, the conductances of both orifices leading to the two chambers will be considered equal and denoted by C, which is assumed to be a function solely of the spool displacement, and ultimately, of the reference voltage.

A black-box approach has been adopted to model the main valve dynamics. The relationship between the reference voltage and the valve conductance is approximated by a second-order transfer function that captures the dominant behavior of the spool dynamics:

$$\frac{\overline{C}}{\overline{V}_{rif}} = \frac{k_v \sigma_n^2}{s^2 + 2\xi_n \sigma_n s + \sigma_n^2} \tag{8}$$

where σ_n is the system's natural frequency, ξ_n is the servovalve damping ratio and the overbar denotes the Laplace transform of the variables. Basing on the previous assumptions a linear static characteristic is assumed between the reference voltage V_{ref} and the valve conductance C:

$$C = k_c x_v = k_c k_s V_{rif} = k_v V_{rif} \tag{9}$$

where $k_v = k_s k_c$, with $k_c = {}^{C_{\max}}/_{x_{v,\max}}$ and $k_s = {}^{x_{v,\max}}/_{V_{rif,\max}}$ respectively the conductance and spool gains.

Therefore, for a given valve conductance C, the flow rate curves of the servovalve orifices connecting the rear and front chambers respectively to the supply and discharge ports are depicted in blue in Figs. 2 and 3. Moreover, it is assumed that the flow conditions remain subsonic for both chambers.

For what concerns the rear chamber, the elliptic flow curve can be linearized with a secant approach, which has the benefit of guaranteeing a null flow for the conditions in which $P_1 = P_s$. An intuitive solution could be to take as second point for the linearization the sonic conditions, that is $P_1 = bP_s$. However, this would lead to a major underestimation of the flow rate along the entire subsonic range. For this reason, a more general approach has been adopted, considering as linearization reference condition a pressure value $P_1 = b_a^* P_s > bP_s$, with $b \leq b_a^* < 1$. As a result, a mean representation of the subsonic section of the flow rate curve is obtained. Figure 2 shows this linear approximation with $b_a^* = 0.5$.

The air flow passing through the servovalve can therefore be expressed as a function of the time-varying conductance C and chamber pressure P_1:

$$G_1' = \frac{\rho_{ANR}}{(1 - b_a^*)} C\,(P_s - P_1) \tag{10}$$

This expression remains non-linear, as it involves the product of two independent variables. Their contributions can be decoupled by applying a Taylor expansion around the linearization point $(b_a^* P_s,\, C_0)$. By linearizing the flow rate entering Chamber 1 in this way, its variations with respect to the operating point are made explicit, leading to the following expression:

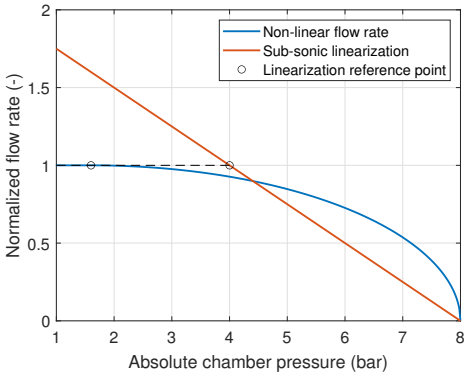

Fig. 2: Linear approximation of the subsonic flow rate chamber charging curve for a given conductance C and a supply absolute pressure of 8 bar, $b = 0.2$ and $b_a^* = 0.5$.

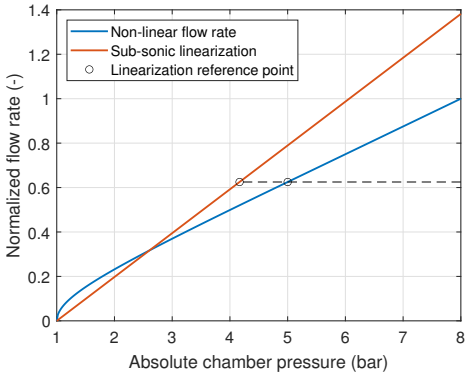

Fig. 3: Linear approximation of the subsonic flow rate chamber discharging curve for a given conductance C and an exhaust absolute pressure of 1 bar, $b = 0.2$ and $b_s^* = 0.24$.

$$\Delta G_1 = G_1' - G_{10}' = G_{Q1}\Delta C + G_{PQ1}\Delta P_1 \tag{11}$$

where G_{Q1} is charging flow gain of the valve, defined as:

$$G_{Q1} = \left.\frac{\partial G_1}{\partial C}\right|_0 = \frac{\rho_{ANR}\,(P_s - P_{10})}{1 - b_a^*} \tag{12}$$

and G_{PQ1} is the charging flow-pressure gain of the valve:

$$G_{PQ1} = \left.\frac{\partial G_1}{\partial P_1}\right|_0 = -\frac{\rho_{ANR} C_0}{1 - b_a^*} \tag{13}$$

The flow gain of the valve represents the variation of flow rate with respect to the spool displacement (or control signal), while the flow-pressure gain defines the sensitivity to variations in the chamber's pressure.

The same approach can be applied to the flow exiting the front chamber toward the exhaust port. However, as shown in Fig. 3, the flow rate does not exhibit a maximum limit corresponding to the choked condition, unlike the flow entering the rear chamber. This behavior is due to the fact that Chamber 2 is discharging, i.e., $P_2 > P_d$, and air flows from the front chamber to the exhaust port. Since the downstream pressure remains constant, the choked flow rate depends on the upstream pressure P_2, and thus continues to increase with it, as described by Eq. (1).

The subsonic section of the non-linear flow rate curve is again approximated with the secant approach, considering as linearization reference point the one defined by a chamber pressure $P_2 = P_d/b_s^*$, with $1 < b_s^* \leq 1/b$. The expression results in:

$$G_2' = \frac{\rho_{ANR} b_s^*}{b\,(1 - b_s^*)} C\,(P_2 - P_d) \tag{14}$$

By applying the Taylor expansion around the linearization point $(P_d/b_s^*,\, C_0)$ the following linear equation is obtained for the flow rate of Chamber 2:

$$\Delta G_2 = G_2' - G_{20}' = G_{Q2}\Delta C + G_{PQ2}\Delta P_2 \tag{15}$$

where G_{Q2} is discharging flow gain of the valve, defined as:

$$G_{Q2} = \left.\frac{\partial G_2}{\partial C}\right|_0 = \frac{\rho_{ANR} b_s^*\,(P_{20} - P_d)}{b\,(1 - b_s^*)} \tag{16}$$

and G_{PQ2} is the discharging flow-pressure gain of the valve:

$$G_{PQ2} = \left.\frac{\partial G_2}{\partial P_2}\right|_0 = \frac{\rho_{ANR} b_s^* C_0}{b\,(1 - b_s^*)} \tag{17}$$

Having linearized the expressions governing the mass flow rates across the valve orifices, attention can now be shifted to the continuity equations describing the pressure dynamics within the cylinder chambers. These equations relate the net mass flow entering or leaving each chamber to the time evolution of pressure, and their linearization is a key step in formulating the complete linear model of the system.

The linearization process of Eqs. (4) - (5) is performed considering a set of boundary conditions and simplifying assumptions, detailed below:

- $T_{1i} = T_{2i} = T$, the initial temperature of the air in both chambers is the same;
- $n = 1$, an isothermal transformation is considered;
- $P_1 = P_{1i} = P_{10}$ and $P_2 = P_{2i} = P_{20}$, the current and initial chambers' pressure coincides with that of the linearization points;
- $\dot{P}_1 = \dot{P}_2 = 0$, the variation of the pressures in both chambers is neglected;
- $x = 0$, the rod is considered in the central position;
- $\dot{x} = \ddot{x} = 0$, the external disturbances are disregarded;
- $F_{fr} = 0$, the friction is neglected.

By applying the first-order Taylor expansion to Eqs. (4) - (5):

$$\Delta G_{1,2} = \left.\frac{\partial G_1}{\partial x}\right|_0 \Delta x + \left.\frac{\partial G_1}{\partial \dot{x}}\right|_0 \Delta \dot{x} + \left.\frac{\partial G_1}{\partial P_1}\right|_0 \Delta P_1 + \left.\frac{\partial G_1}{\partial \dot{P}_1}\right|_0 \Delta \dot{P}_1 \tag{18}$$

the following equations can be obtained for the mass flow rate of both chambers:

$$\Delta G_1 = \frac{P_{10} A_1}{RT}\Delta \dot{x} + \frac{A_1 x_0}{RT}\Delta \dot{P}_1 \tag{19}$$

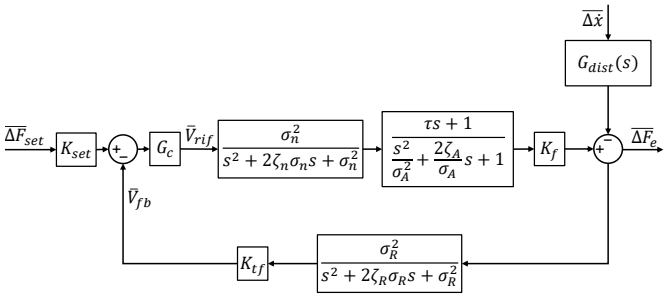

Fig. 4: Reduced block diagram of the linearized model.

$$\Delta G_2 = \frac{P_{20}A_2}{RT}\Delta\dot{x} - \frac{A_2 x_0}{RT}\Delta\dot{P}_2 \tag{20}$$

By equating the flow rate expressions on the servovalve side (Eqs. (11) - (15)) and actuator side (Eqs. (19) - (20)), it is possible to derive the resulting expression for the chamber pressures, which can now be incorporated into the rod equilibrium equation, expressed with an incremental notation with respect to the reference point:

$$\Delta F_e = F_e + F_{e0} = \Delta P_1 A_1 - \Delta P_2 A_2 - M\Delta\ddot{x} - \gamma\Delta\dot{x} \tag{21}$$

According to the previous assumptions, it is possible to simplify the last two terms such that $M\Delta\ddot{x} = M\ddot{x}$ and $\gamma\Delta\dot{x} = \gamma\dot{x}$.

After transforming and combining the equations presented so far into the Laplace domain, and performing a series of algebraic manipulations, the block diagram shown in Fig. 4 can be obtained. It is mainly composed of three main transfer function relative to the system (the servovalve, the actuator and the force sensor), a transfer function G_c containing the regulator logic (for the time being, a simple PI controller) and two independent static gains, $K_{set} = K_{tf}$ and K_f. The latter contains all the static gains of the main upper branch of the block diagram, and is expressed as:

$$K_f = \frac{k_v\left[A_1\left(P_s - P_{10}\right) + A_2\left(P_{20} - P_d\right)\right]}{C_0} \tag{22}$$

The transfer function of the actuator exhibits a first-order zero with time constant τ, defined as:

$$\tau = \frac{A_1 A_2 w\left[\left(P_s - P_{10}\right)\frac{(1-b_s^*)b}{b_s^*} + \left(P_{20} - P_d\right)\left(1 - b_a^*\right)\right]}{\rho_{ANR}C_0\left[A_1\left(P_s - P_{10}\right) + A_2\left(P_{20} - P_d\right)\right]} \tag{23}$$

with $w = {}^{(x_0 + x_m)}/_{nRT}$. The denominator is of second order, with a natural frequency σ_A and a damping ratio ξ_A, expressed as follows:

$$\sigma_A = \frac{\rho_{ANR}C_0}{w}\sqrt{\frac{b_s^*}{A_1 A_2 b\left(1 - b_a^*\right)\left(1 - b_s^*\right)}} \tag{24}$$

$$\xi_A = \frac{1}{2}\frac{A_1\frac{b_s^*(1-b_a^*)}{b} + A_2\left(1 - b_s^*\right)}{\sqrt{\frac{b_s^* A_1 A_2}{b}\left(1 - b_a^*\right)\left(1 - b_s^*\right)}} \tag{25}$$

The feedback branch of the block diagram shows a black-box representation of the force sensor and its conditioning system, characterized by a natural frequency σ_R, a damping ratio ξ_R and a static gain $K_{tf} = {}^{V_{fb,\max}}/_{F_{e,\max}}$.

Finally, the force closed loop is closed by setting up the following expression:

$$\overline{V}_{rif} = G_c\left(\overline{V}_{set} - \overline{V}_{fb}\right) \tag{26}$$

with $\overline{V}_{set} = K_{set}\overline{\Delta F}_{set}$ and $\overline{V}_{fb} = K_{tf}\overline{\Delta F}_e$ for $s \to 0$.

The disturbance transfer function is not explicitly represented for the sake of readability and as it falls outside the scope of the present work.

V. Results and Discussion

The equations presented in Section III have been implemented within the reference non-linear model of the servosystem, whose main interface is shown in Fig. 5. The model was developed in the MATLAB/Simulink R2024b environment and integrated using the ode1be solver with a sampling frequency of 100 kHz. It has been employed as a virtual test bench to provide a preliminary verification of the consistency between the linearized model and the non-linear system behavior.

In this section, a comparison is presented between the frequency responses obtained from the detailed non-linear model and its linearized counterpart. The aim is to evaluate the accuracy and reliability of the linear approximation in capturing the dynamic behavior of the system under realistic, yet non-extreme, operating conditions.

With this aim, a sinusoidal input force with a peak amplitude of 1000 N is commanded. This value corresponds to approximately 7% of the actuator's stall load and was deliberately selected to avoid the onset of significant non-linear phenomena, such as power saturation or other amplitude-dependent nonlinearities, which would otherwise compromise the validity of the comparison and distort the frequency response of the non-linear model, shifting its working conditions far from the linearization point. By maintaining the excitation amplitude at a sufficiently low level, the comparison between the two models becomes meaningful, and the response of the linear system can be reasonably expected to align with that of the non-linear model in terms of both amplitude and phase over a range of input frequencies. The following analysis aims to demonstrate the applicability of the linear model for control

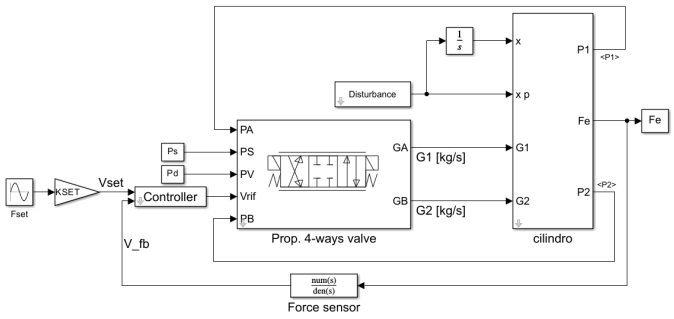

Fig. 5: Non-linear dynamic reference model.

design purposes, within a defined region around the selected operating point. The main parameters of the considered force-controlled servosystem, installed on the test bench of Fig. 1, are retrieved from manufacturers' catalogues and experimental literature's studies [11] and listed in Tab. I.

The comparison between the frequency responses of the linear and non-linear models is presented in Fig. 6. As shown, the linearized model accurately captures the key dynamic features of the system. In particular, a strong agreement is observed between the two responses, especially in the frequency range of interest, i.e. in the vicinity of the system's cut-off frequency.

Moreover, the results clearly highlight that there is still room for improvement in terms of control performance and bandwidth enhancement. The good correspondence between the linear and non-linear models across a wide frequency range allows stability and control analyses to be carried out with confidence. Indeed, since both models exhibit comparable behavior under the same excitation conditions, the linear approximation can be reliably used to guide control design decisions. The stability margins of the system can be extracted from the picture, resulting in an open loop gain margin of 17.5 dB at $\omega = 35.4$ rad s^{-1}, and an open loop phase margin of 87.5 deg at $\omega = 442$ rad s^{-1}. This results in a close loop bandwidth of approximately 6.8 Hz. It is worth noting that the objective of this analysis is to validate the linear model against the non-linear benchmark. For this reason, both models share the same set of control parameters, which are not yet optimized. These parameters will be refined in the final implementation phase on the physical test bench.

VI. Conclusions

This paper presents a design methodology for a pneumatic force-control servo system, based on the comparison between an original linearized model and a high-fidelity nonlinear model. The linearized, fully parametric formulation delivers effective results, as demonstrated by the good agreement in the frequency response over a wide range of operating frequencies.

Future developments will focus on leveraging the linearized model to assess the feasibility of more advanced control strategies (e.g. MPC or SMC), investigating the impact of external speed disturbances, performing a sensitivity analysis on the results with respect to different linearization points, and validating the model against experimental data collected from the test bench.

TABLE I: Servosystem's main parameters.

Property	Symbol	Unit	Value
Supply absolute pressure	P_s	bar	8
Exhaust absolute pressure	P_d	bar	1
Maximum voltage	$V_{rif,\max}$	V	10
Valve's critical pressure ratio	b	-	0.2
Valve's sonic conductance	$C_{\max}$	m^3/(s Pa)	9×10^{-8}
Charging lin. pressure ratio	b_a^*	-	0.5
Discharging lin. pressure ratio	b_s^*	-	0.24
Linearization conductance	C_0	m^3/(s Pa)	$C_{\max}/2$
Valve's natural frequency	σ_n	rad s^{-1}	440
Piston bore	D	mm	160
Actuator total stroke	L	mm	350
Actuator's stall force	$F_{e,\max}$	kN	14.1

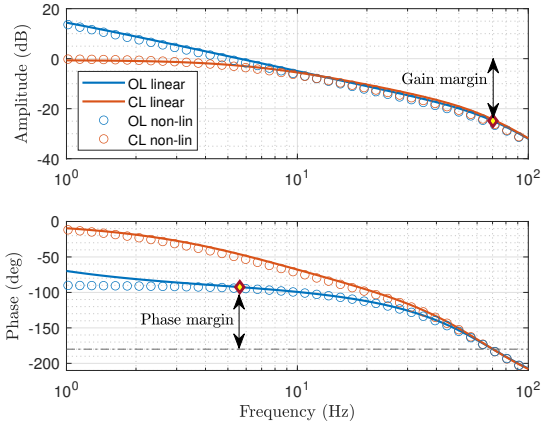

Fig. 6: Comparison between the force frequency responses obtained from the linear and non-linear models with 1000 N set amplitude.

CRediT author contributions

CRediT author contributions: A.C.B.: conceptualization; data curation; formal analysis; investigation; methodology; software; validation; visualization; writing—original draft; writing—review and editing. **A.D.M.**: conceptualization; validation. **M.S.**: conceptualization; methodology; funding acquisition; supervision.

All authors have read and agreed to the manuscript published version.

References

[1] K. Khayati, P. Bigras, and L.-A. Dessaint, "A robust feedback linearization force control of a pneumatic actuator," in *2004 IEEE International Conference on Systems, Man and Cybernetics*, vol. 7. IEEE, 2004, pp. 6113–6119.

[2] D. Saravanakumar, B. Mohan, and T. Muthuramalingam, "A review on recent research trends in servo pneumatic positioning systems," *Precision Engineering*, vol. 49, pp. 481–492, jul 2017.

[3] K. Kawashima, T. Fujita, and T. Kagawa, "The Effect of Nonlinear Characteristics on Pneumatic Servo Systems," *Proc. of the JFPS Int. Symposium on Fluid Power*, vol. 1999, no. 4, pp. 137–142, 1999.

[4] T. Hashimoto and Y. Ishida, "An adaptive I-PD controller based on frequency domain system identification," *ISA Transactions*, vol. 39, no. 1, pp. 71–78, feb 2000.

[5] H. I. Ali, S. B. B. Noor, S. M. Bashi, and M. H. Marhaban, "A review of pneumatic actuators (Modeling and control)," *Australian Journal of Basic and Applied Sciences*, vol. 3, no. 2, pp. 440–454, 2009.

[6] A. C. Bertolino, A. De Martin, M. Gaidano, S. Mauro, and M. Sorli, "A fully sensorized test bench for prognostic activities on ball screws," in *ICECCME 2021*, no. October, 2021, pp. 7–8.

[7] M. Sorli, G. Figliolini, and A. Almondo, "Mechatronic Model and Experimental Validation of a Pneumatic Servo-Solenoid Valve," *J. of Dyn. Sys., Meas., and Control*, vol. 132, no. 5, pp. 1–10, sep 2010.

[8] ISO 6358-1:2013, "Pneumatic fluid power - Determination of flow-rate characteristics of components using compressible fluids - Part 1: General rules and test methods for steady-state flow," 2013.

[9] D. Zhang, L. Gao, S. Zhou, Y. Ma, and B. Li, "Measurement of the mass-flow-rate characterization parameters of high-pressure pneumatic servo slide valves," *Scientific Reports*, vol. 12, no. 1, pp. 1–11, 2022.

[10] H. E. Merrit, *Hydraulic Control Systems*, I. John Wiley & Sons, Ed. New York, London, Sydney: John Wiley & Sons, Inc., 1967.

[11] J. Pérez García, I. Murcia Murcia, A. Fernández Jiménez, and A. Viedma Robles, "Compressible bench flow adaptations to the experimental characterization of pneumatic fluid power components. Application to the determination of flow-rate characteristics of a Festo MPYE-5-3/8-010-B proportional valve," in *3rd FPNI-PhD Symposium on Fluid Power*, Terrassa, Spain, 2004, pp. 1–15.